Structural Response of Materials Due to In-Depth Heating

J. A. Nemes* and C. I. Chang†
Naval Research Laboratory, Washington, D.C.

The effect of uniform through-thickness energy deposition on the thermal-mechanical response of several structural materials is evaluated. Expressions used for determining temperature distributions under moderate deposition rates are presented. Temperature histories of aluminum, titanium, and graphite-epoxy panels subject to electron beam irradiation are compared with analytical results to assess the validity of the methods used. Dynamic material response under extreme deposition rates are developed for instantaneous and finite pulse deposition. Expressions for determining the regime of dominant thermal or dynamic response are given as a function of total energy and energy deposition rate.

Introduction

DIRECTED energy weapons considered under the Strategic Defense Initiative include chemical lasers, excimer lasers, x-ray lasers, particle beam weapons, and kinetic energy weapons.[1] These weapons can be divided into those that deposit energy primarily at the target surface and those that deposit energy through the thickness of the material. The latter group is the focus of this paper. Both these categories can be further subdivided based on their rate of deposition. Although all these weapons would obviously deposit energy in a relatively short time, the terms "slow deposition" and "rapid deposition" are used to distinguish among effects. With rapid deposition, dynamic effects dominate the response whereas, in slow deposition, dynamic effects can be considered negligible. The difference in the means of energy deposition obviously affects the thermal and mechanical response of structural materials, which in turn strongly influences the type of failure that would be induced in a potential target.

Under rapid energy deposition rates, tremendous compressive stresses are initially induced in the material. However, in order to maintain the stress-free conditions at the boundary, release waves propagate into the material, resulting in correspondingly large tensile stresses. Although the stress distributions due to in-depth and surface deposition differ, the types of failure induced do not differ significantly. In metals, if the tensile stresses generated are sufficiently large, spallation failure, in which the material is "blown apart," occurs. In composite materials, the tendency would be for severe delamination to occur since the interlaminar strength, in general, would be the weakest part of the composite.

In the absence of dynamic effects, materials subjected to slow energy deposition are characterized by a dominant thermal response. Although this is applicable both when energy is deposited on the surface and when it is deposited through thickness, there are distinctions to be noted. In the case of surface deposition, heat is concentrated over a very thin layer, with little conduction through the thickness taking place during the short time period of interest. As such, the temperature of this layer is increased rapidly until the melting point of metals or the sublimation point of polymers is reached. Further input of energy results in the phase change and removal of the material. This mechanism then enables energy to be transferred to a greater depth within the material, thus providing an alternate to the conduction mechanism for transferring heat. With this type of material response to energy deposition at slow rates, structural failure therefore occurs primarily through material removal. The thermal-mechanical response of simple metal structures subject to surface heating has been studied in Ref. 2. References 3 and 4 discuss the effect of surface heating on composite materials. Numerous other references on the topic can also be found.

In contrast to the failure process due to surface energy deposition is that which occurs when structures are subjected to in-depth heating at slow rates. Since there is essentially uniform heating through the thickness of the material, structural failure is usually induced before the melting or sublimation temperature is reached. Failure is instead caused by degradation of mechanical properties with increasing temperatures. The reduction in a material's ultimate strength will lead to loss of load-carrying ability of tensile members or burst in pressure vessels. Similarly, reduction of modulus with increasing temperature will result in buckling of structures subject to compression.

Slow Energy Deposition

As stated previously, the predominant effect of energy deposition at slow rates is increase in material temperature. We, therefore, consider initially the governing heat conduction equation in its most general form. The equation in a Cartesian coordinate system is[5]

$$\rho c \frac{\partial T}{\partial t} = \frac{\partial}{\partial x}\left(K_x \frac{\partial T}{\partial x}\right) + \frac{\partial}{\partial y}\left(K_y \frac{\partial T}{\partial y}\right) + \frac{\partial}{\partial z}\left(K_z \frac{\partial T}{\partial z}\right) + A(x, y, z, t) \tag{1}$$

where ρ is the material density, c the specific heat, T the temperature, t the time, A the additional heat source term, and K_x, K_y, K_z the conductivities in the x, y, z directions. It should be noted that, in general, ρ, c, and K are functions of temperature.

Boundary conditions are usually specified in terms of heat flux along a boundary surface such that

$$\frac{\partial T}{\partial x} = f_1(y, z, t)$$

$$\frac{\partial T}{\partial y} = f_2(x, z, t)$$

$$\frac{\partial T}{\partial z} = f_3(x, y, t) \tag{2}$$

Initial conditions are defined in terms of initial temperature, usually constant,

$$T(x, y, z) = T_0 = \text{const} \; @ \; t = 0 \tag{3}$$

Received April 14, 1986; revision received Aug. 29, 1986.

*Mechanical Engineer, Structural Integrity Branch.
†Branch Head, Structural Integrity Branch.

Boundary conditions normally specified include those to account for convective and radiation losses. Considering losses from the z face, $f_3(x, y, t)$ takes the following form:

$$f_3(x, y, t) = h(T - T_r) + \sigma\epsilon(T^4 - T_0^4) \tag{4}$$

where h is the convection coefficient, T_r the recovery temperature, σ the Stefan-Boltzmann constant, ϵ the emissivity, and T_0 the ambient temperature.

In order to define A in Eq. (1) for the specific case in which in-depth heating is due to particle beam irradiation, some additional relations must be introduced. The passage of fast-moving charged particles through a material produces a number of physical reactions. It is of primary interest, however, that the charged particles lose energy principally by inelastic collisions with atoms in the target material.[6,7] The average energy loss per unit path length is called the stopping power S, which is defined as

$$S = -1/\rho \frac{dE}{dx} \tag{5}$$

The units of S are expressed in terms of MeV cm^2/g. If we then consider the number of charged particles passing per unit area, per unit time as the current density j, we can define the energy per unit mass given up by a pulse of charged particles as follows:

$$\Delta E_p = j\tau_p S \tag{6}$$

where τ_p is the pulse length. Then assuming that the temperature variation between pulses can be neglected, A, over the irradiated area for a uniform pulse, can be computed simply as

$$A = \Delta E_p f \rho \tag{7}$$

where f is the pulse rate. The above formulas are based on the assumption that the charged particles have passed through the material. This assumption is obviously valid for thin foils. Determination of its limit of applicability is based on the range r_0 of the charged particle.[7] The range represents the average path length traveled by a particle as it slows down from an initial energy E_i to final energy E_f. Reference 8 tabulates stopping powers and ranges for a number of materials. Table 1 shows both the stopping power and the range for three materials subject to electron beams at two energy levels. As can be seen from the table, the primary difference between the two energy levels is in the range of the particle, with little variation in the stopping power. Thus, for material thicknesses less than this range, the heat per unit mass is essentially constant.

As the simplest case, we consider a beam of charged particles directed along the z axis. If the distribution of particles is constant in the x–y plane and the losses from convection and radiation are negligible, then Eq. (1) is simply reduced to a volume subject to a constant heat source resulting in a linearly increasing temperature. A more realistic case, however, is a beam distribution constant in time but with a spatial variation in the x–y plane. If we consider this to be a Gaussian distribution, we can consider Eqs. (1) and (2) in an axisymmetric form as shown:

$$\rho c \frac{\partial T}{\partial t} = 1/r \frac{\partial}{\partial r}\left[K_r\left(r\frac{\partial T}{\partial r}\right)\right] + \frac{\partial}{\partial z}\left(K_z \frac{\partial T}{\partial z}\right) + A(r, t) \tag{8}$$

$$\frac{\partial T}{\partial z} = f_1(r, t), \qquad \frac{\partial T}{\partial r} = f_2(z, t) \tag{9}$$

Consideration of temperature-dependent properties K_r, K_z, ρ, and c requires that Eqs. (8) and (9) be solved numerically. Note that in Eq. (8), the gradient in the z direction is due to the surface losses.

Table 1 Comparison of stopping power and particle range at two energy levels

	Stopping powers MeV-cm^2/g		Range, cm	
Material	20 MeV	40 MeV	20 MeV	40 MeV
Aluminum	1.707	1.770	3.913	6.628
Titanium	1.584	1.648	2.326	3.742
Graphite	1.816	1.877	6.229	11.16

Description of Experiment

Samples of aluminum, titanium, and graphite-epoxy were subjected to electron beam irradiation at the Naval Research Laboratory linear accelerator (Linac). The purpose of the experiments was to verify that the theory presented in the previous section sufficiently describes the thermal response of the material for the purpose of performing structural evaluation. The specimens used were 7.62 cm × 7.62 cm × 0.635 cm, with the beam directed through the thickness. All specimens were instrumented with thermocouples using a number of different configurations. Specimens were tested at both the 20-MeV and 40-MeV level. The length of exposure varied with each test. Film dosimetry was used to determine the spatial distribution of particles. This normalized distribution is shown in Fig. 1. The beam consisted of 360 pulses/s, with each pulse being 300 mA with duration of 1.5 μs. Specific alloys tested were 6061-T6 aluminum and 6AL-4V titanium. The graphite-epoxy tested was AS4/3501-6 and was composed of 0° and $\pm 68\frac{1}{2}^\circ$ layers. Using laminate notation, the lay-up is expressed as $[0_8/\pm(68\frac{1}{2})_3/0_8/\pm(68\frac{1}{2})_3]_s$.

Experimental Results

The thermal response of the specimens was recorded by sampling the thermocouples at 10 Hz per channel. Temperature time histories were produced for each of the materials tested. Due to the high conductivity, heat is conducted away from the center rapidly in the aluminum sample, thus requiring a large number of pulses to reach the melting temperature. In contrast, titanium, with a much lower diffusivity, reached melting temperature in a shorter number of pulses. Post-test examination of metal specimens showed evidence of melting, although a much smaller area was involved in the case of titanium. The testing of graphite-epoxy specimens, witnessed through TV monitors, showed that pyrolysis of the epoxy resin began almost instantaneously upon heating. Specimens that were subject to irradiation for long times (100 s) showed damage over the entire specimen, including delamination of the corner of the

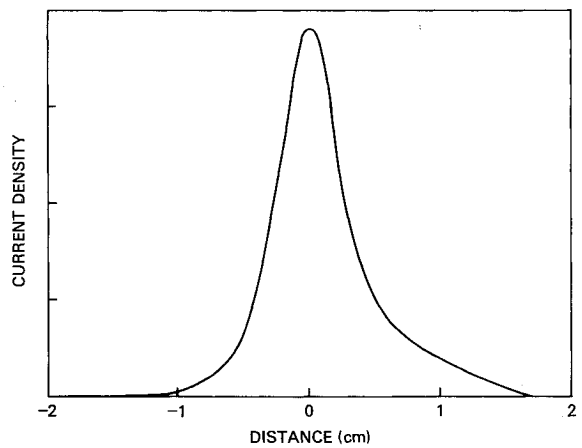

Fig. 1 Particle distribution at 40 MeV.

specimen. This appearance of delamination seems to be associated with hot-gas buildup within the specimen.

Experiments conducted at 20 MeV and 40 MeV showed little variation in the resulting temperature field, as would be expected from the small difference in stopping powers at the two energy levels for a given material.

Analytical Results

The correlation of theory with experimental results requires that Eqs. (8) and (9) be solved. Since the temperature range of the response is wide, the variation of the thermophysical properties K and c must be considered. Numerical techniques are therefore required for solution of the problem.

A finite-difference axisymmetric computer code has been developed to determine solutions to Eqs. (8) and (9). The difference expressions are developed by considering the energy balance of a differential element subject to a volumetric heat source. Conditions at the boundary consider losses from convection and radiation. Temperature-varying properties are also considered. The time increment used in solving the expressions must be small enough to maintain stability. Stability requirements for finite-difference expressions are given in a number of texts on numerical techniques, such as Ref. 9.

Thermophysical properties for the metals were obtained from Ref. 10. Properties for the graphite-epoxy material are, however, not as well defined over the temperature range of interest. Heat capacity for the composite material can be expressed from the properties of the constituents

$$C_c = V_f C_f + V_m C_m \tag{10}$$

where C_c, C_f, C_m are the heat capacity of the composite, fiber, and matrix material, respectively, and V_f and V_m represent the volume fraction of the constituents. Although Eq. (10) gives a theoretical expression for heat capacity of the composite, the problem remains, since the temperature variation of heat capacity for the graphite fiber and epoxy are also not well defined. The heat capacity used in the numerical analysis is shown in Fig. 2. The spike in the curve from 400 to 480°C represents the heat absorbed in the pyrolysis of the epoxy.

The conductivity for graphite-epoxy must also consider the anisotropy of the material in addition to the heterogeneity. Although expressions for conductivity based on volume fraction similar to Eq. (10) are possible, more data are available on conductivity of the composite. Individual lamina conductivities are taken along the fiber, through thickness, and across transverse directions. To perform the numerical analysis, it is necessary to transform the in-plane conductivities into global coordinates as follows:

$$\begin{Bmatrix} K_L \\ K_T \\ K_{LT} \end{Bmatrix} = \begin{bmatrix} \cos^2\theta & \sin^2\theta & -2\sin\theta\cos\theta \\ \sin^2\theta & \cos^2\theta & 2\sin\theta\cos\theta \\ \sin\theta\cos\theta & -\sin\theta\cos\theta & \cos^2\theta - \sin^2\theta \end{bmatrix} \begin{Bmatrix} K_f \\ K_t \\ 0 \end{Bmatrix} \tag{11}$$

where K_L is the conductivity corresponding to the 0° direction, and K_T in the in-plane transverse direction. K_f and K_t are conductivities in the lamina coordinates. Therefore, from Eq. (11),

$$K_L = \sum_{i=1}^{n} (\cos^2\theta_i K_f + \sin^2\theta_i K_t) \Big/ n$$

$$K_T = \sum_{i=1}^{n} (\sin^2\theta_i K_f + \cos^2\theta_i K_t) \Big/ n$$

$$K_{LT} = \sum_{i=1}^{n} (\sin\theta\cos\theta K_f - \sin\theta\cos\theta K_t) \Big/ n \tag{12}$$

where summation is for n layers. Since the laminate being considered has $+\theta$ and $-\theta$ layers, the cross-conductivity term K_{LT} reduces to zero. In order to reduce the problem to two dimensions to simplify the calculations, it is necessary to define a single radial conductivity independent of θ. As such, the following approximation is used: the radial conductivity K_r is the average of K_L and K_T. The resulting radial conductivity is shown in Fig. 3. In the thickness direction, the conductivity K_z is equal to the through-thickness lamina value.

Numerical analysis was performed for all three materials at both energy levels. Comparisons were made between the analytical results and the corresponding thermocouples. Figure 4 shows the comparison for individual points on the specimen. In general, the correlation was very good for the metals. Some discrepancy was found for the graphite-epoxy. Based on the lack of definite material properties and assumptions required to perform an axisymmetric analysis, such discrepancy was to be expected.

From the figures it can be seen that the theory presented earlier adequately described the thermal response of material to particle-beam irradiation. Using these temperature time histories, it would then be possible to determine mechanical response of simple structures. Consideration of stress redistribution due to temperature-varying mechanical properties along with stresses induced by restraint of thermal expansion could be found utilizing finite-element or other numerical tech-

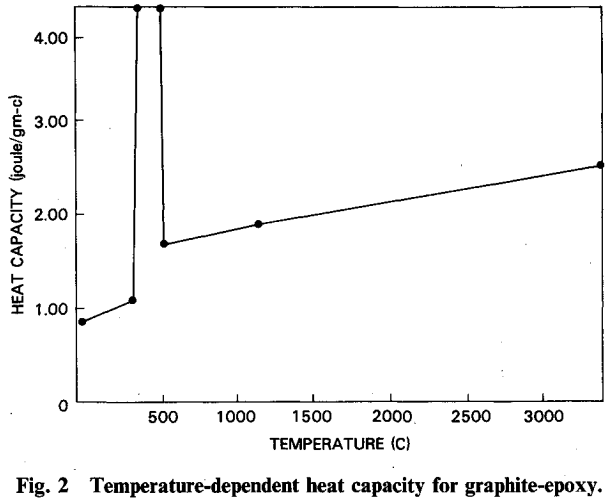

Fig. 2 Temperature-dependent heat capacity for graphite-epoxy.

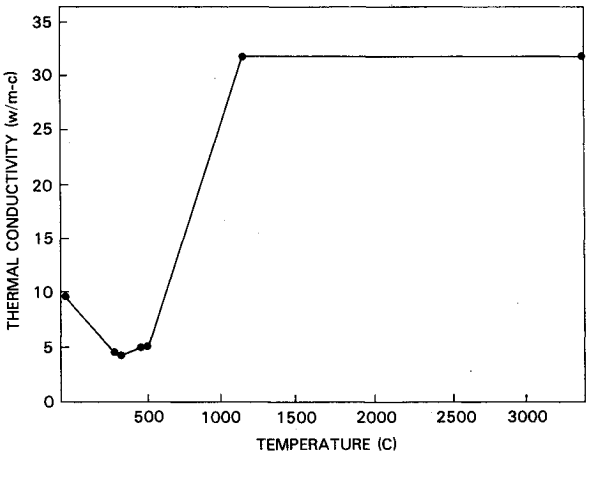

Fig. 3 Temperature-dependent radial thermal conductivity for graphite-epoxy.

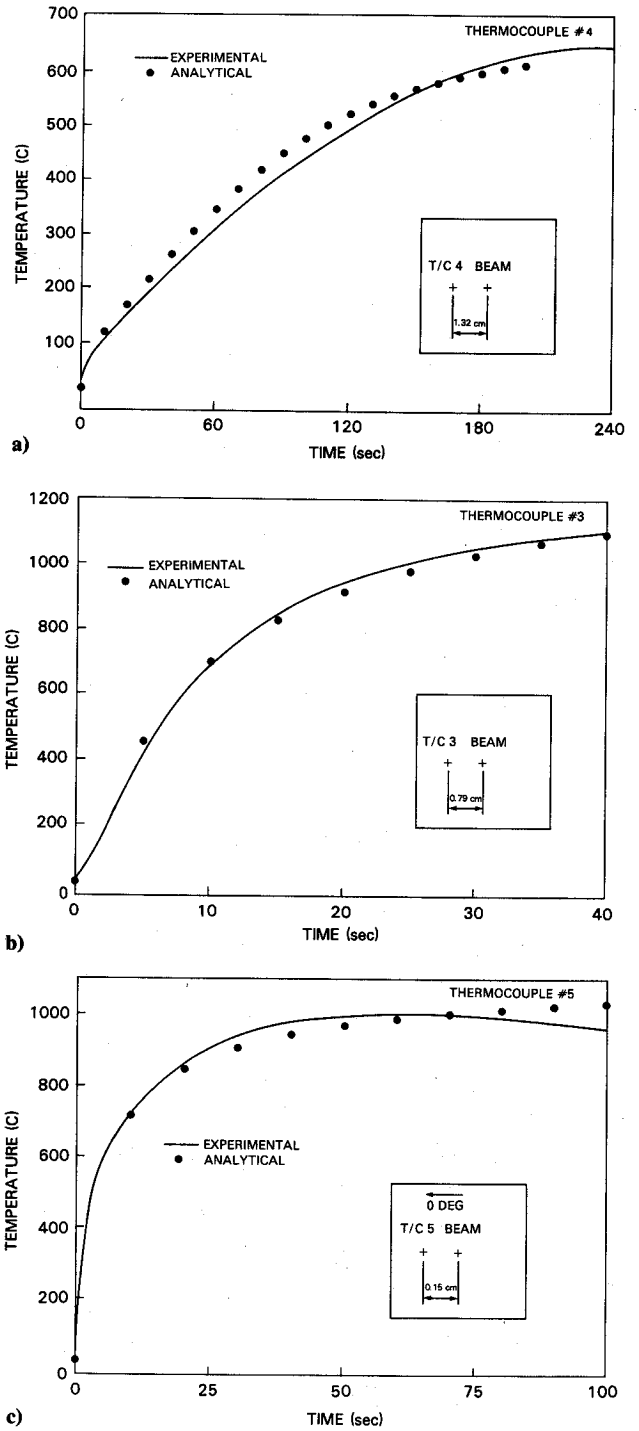

Fig. 4 Comparison of analytical to experimental results for a) aluminum, b) titanium, and c) graphite-epoxy.

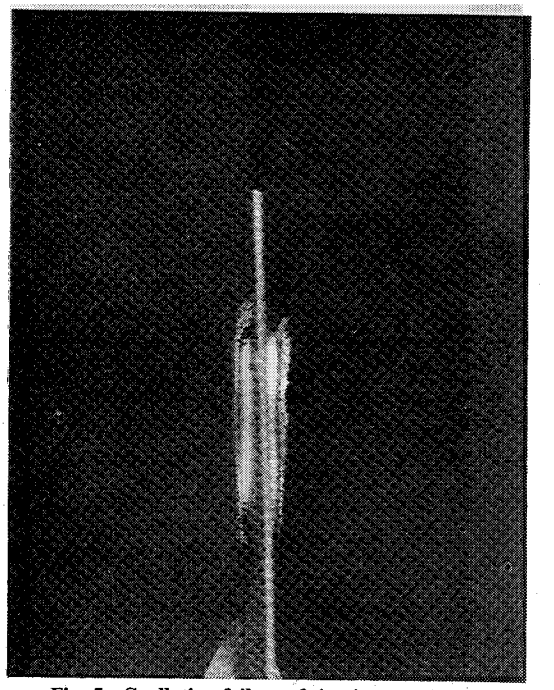

Fig. 5 Spallation failure of titanium specimen.

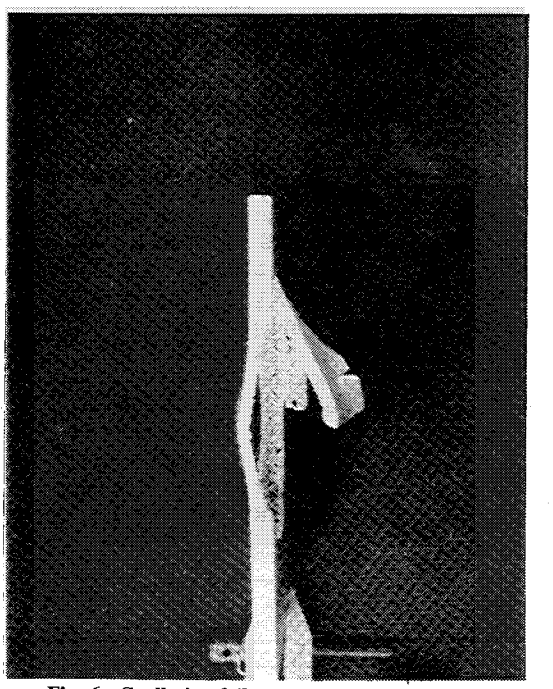

Fig. 6 Spallation failure of aluminum specimen.

niques. In addition, after selection of appropriate failure criteria and consideration of the material's temperature-dependent strengths, it would be possible to determine integrity of structures subject to particle beam irradiation.

Rapid Energy Deposition

In this section, the response of material subjected to in-depth energy deposition at extremely high rates will be discussed. At high deposition rates, stresses and dynamic effects in the material are significant in comparison with the low deposition rates previously discussed. It is therefore necessary to develop relations to express the time-varying nature of these stresses so that the material response can be studied. If the tensile stresses generated in the material are sufficiently large, the material may fail by spallation, which actually splits the material apart. Spallation failures of titanium and aluminum specimens are shown in Figs. 5 and 6. As seen in the figures, the material has failed with symmetry about the centerline. This is characteristic of uniform in-depth energy deposition. Spallation failures generated from surface or nonuniform energy deposition may exhibit spall planes at locations other than the centerline or may have separate spall planes near the front and back surfaces.

Development

In order to develop analytical expressions for stresses as a function of time, there are a number of assumptions used to simplify the problem, which is shown schematically in Fig. 7.

We consider a plate of thickness h, subjected to incident energy directed along the x axis. The energy distribution is uniform in thickness over a finite area of the y–z plane. At the time periods of interest, which for thin specimens is of the order of several hundred nanoseconds to several microseconds, the heat conduction away from the area subjected to the incident energy is negligible. In addition, we also assume that the diameter of the energy zone is several times larger than the thickness of the specimen. As such, the interaction of relief waves in the y–z plane will not strongly alter the one-dimensional stress waves in the x direction. With these assumptions, we are able to consider one-dimensional expressions for determination of stresses.

In the development to follow, an approximate equation of state relating stresses to strains and internal energy will be used. This relation, in general, is nonlinear over the stress range that will be considered. Again, however, in the interest of developing relatively simplified governing equations, we consider the stress to be expressed in a linear form as follows:

$$\sigma \cong E_0 \frac{\partial u}{\partial x} - \Gamma \rho \epsilon \tag{13}$$

where E_0 is the confined modulus of the material, u the x-direction displacement, Γ the Grüneisen ratio, ρ the deformed density of the material, and ϵ the internal energy. The Grüneisen ratio is further defined as

$$\Gamma = \frac{\alpha k}{\rho c_v} \tag{14}$$

where α is the coefficient of thermal expansion, c_v the material heat capacity at constant volume, and k the bulk modulus.

As a bounding case, we consider the situation in which energy is deposited instantaneously into a material. This instantaneous energy deposition causes heating of the material which, under the inertially restrained conditions we have assumed, results in uniform compression stresses through the thickness of the material. This uniform compression, which is taken as the initial stress condition, can be computed directly from Eq. (13) with $\partial u/\partial x = 0$. For times $t \geq 0$, we have the stress-free conditions at the boundary, which are written as

$$\sigma\left(\frac{-h}{2}, t\right) = \sigma\left(\frac{h}{2}, t\right) = 0 \tag{15}$$

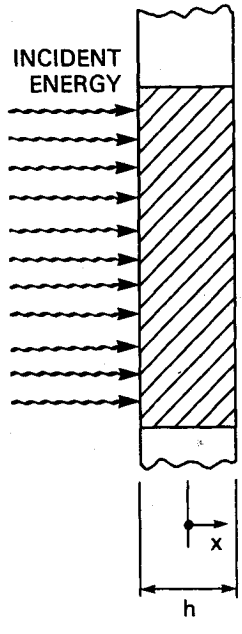

Fig. 7 Schematic representation of a thin plate subjected to rapid energy deposition.

In addition to these conditions, we are also able to take advantage of symmetry about the centerline, which yields the condition

$$u(0, t) = 0 \tag{16}$$

Therefore, for $t \geq 0$, release waves propagate from each surface to maintain the conditions in Eq. (15). As these waves propagate toward the centerline, the material ahead of the waves remains in the initial compressive state, with that behind the wave transformed to a stress-free state. As these waves reach the centerline, their superposition results in tensile stresses of a magnitude equal to the initial compressive stresses. If these stresses are greater than the spallation strength of the material, spallation failure occurs. At stress levels below that, the material undergoes alternating tensile and compressive states until damping mechanisms reduce the stress levels to zero, and the problem is therefore reduced to a heat conduction problem as previously discussed. It should be stated that since we are primarily interested in maximum tensile stresses, which occur during the first cycle, the damping mechanisms are not required in the development.

As can be seen, the computation of maximum tensile stress under the assumption of instantaneous in-depth energy deposition is relatively straightforward. We are, however, interested in the case in which the energy is deposited over a finite period of time. In particular, we want to define material response as a function of energy deposition rate.

In order to develop these relations, it is first necessary to define the one-dimensional momentum balance and energy bal-

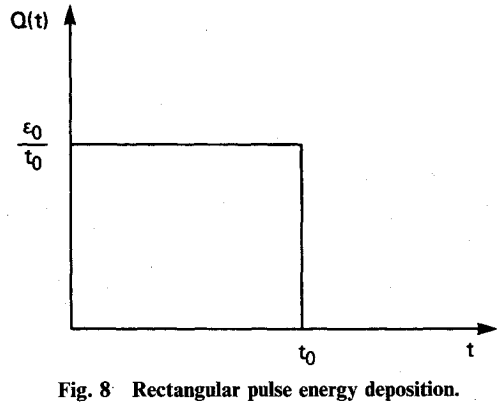

Fig. 8 Rectangular pulse energy deposition.

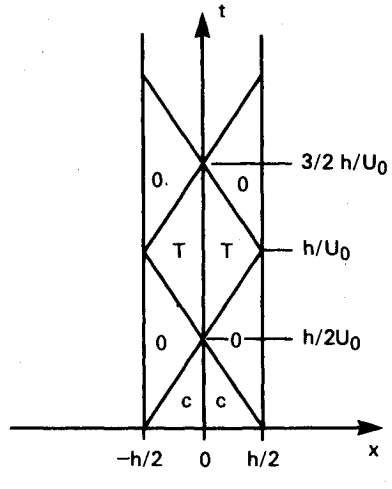

Fig. 9 Stress in different zones of a plate subject to in-depth energy deposition over finite time (T) tension, (c) compression, and (0) stress-free.

ance expressions, which are given below:

$$\rho \frac{\partial^2 u}{\partial t^2} = \frac{\partial \sigma}{\partial x} \tag{17}$$

$$\frac{\partial \epsilon}{\partial t} = 1/\rho_0 \sigma \frac{\partial^2 u}{\partial x\, \partial t} + 1/\rho \frac{\partial q}{\partial x} + Q(t) \tag{18}$$

in which the term ρ_0 is the initial density of the material. In the remaining discussion, the deformed density ρ will be taken as equal to the initial density ρ_0. The first term on the right side of Eq. (18) represents the strain energy rate, and the second represents the heat conduction rate. In view of assumptions previously identified, both of these terms are small in comparison with the energy deposited in the material. Thus, Eq. (18) can be written simply as

$$\frac{\partial \epsilon}{\partial t} = Q(t) \tag{19}$$

$Q(t)$ represents the energy deposition as a function of time. For example, if we consider a rectangular pulse, the energy deposition will be as shown in Fig. 8. This can be represented by the function

$$Q(t) = \epsilon_0/t_0[H(t) - H(t - t_0)] \tag{20}$$

where $H(\ )$ is the Heaviside step function

$$H(x - x_0) = 1 \text{ for } x \geq x_0$$

$$H(x - x_0) = 0 \text{ for } x < x_0$$

Using the equation of state (13), the momentum balance (17) can be given in the form

$$\rho_0 \frac{\partial^2 u}{\partial t^2} = E_0 \frac{\partial^2 u}{\partial x^2} - \Gamma \rho_0 \frac{\partial \epsilon}{\partial x} \tag{21}$$

Since we are considering uniform energy deposition, $\partial\epsilon/\partial x$ is equal to zero, and Eq. (21) reduces to the simple wave equation

$$\frac{\partial^2 u}{\partial t^2} = U_0^2 \frac{\partial^2 u}{\partial x^2} \tag{22}$$

where the wave velocity $U_0 = \sqrt{E_0/\rho_0}$.

We therefore seek solutions in the form

$$u(x, t) = -f\left(t - \frac{(x + h/2)}{U_0}\right) + f\left(t + \frac{(x - h/2)}{U_0}\right) \tag{23}$$

Considering the boundary conditions in Eqs. (15) and (16) and energy deposition defined by Eq. (20), the solution is found to be defined by

$$f(t) = \frac{U_0 \Gamma \rho_0 \epsilon_0}{2E_0 t_0}[t^2 H(t) - (t - t_0)^2 H(t - t_0)] \tag{24}$$

With this expression for $f(t)$, displacements, strains, and stresses can be determined. The expression for stresses that will be used subsequently is given below:

$$\begin{aligned}\sigma(x, t) = \frac{\Gamma \rho_0 \epsilon_0}{t_0} \Bigg\{ &\left[t + \frac{(x - h/2)}{U_0}\right] H\left[t + \frac{(x - h/2)}{U_0}\right] \\ &- \left[t - t_0 + \frac{(x - h/2)}{U_0}\right] H\left[t - t_0 + \frac{(x - h/2)}{U_0}\right] \\ &+ \left[t - \frac{(x + h/2)}{U_0}\right] H\left[t - \frac{(x + h/2)}{U_0}\right] \\ &- \left[t - t_0 - \frac{(x + h/2)}{U_0}\right] H\left[t - t_0 - \frac{(x + h/2)}{U_0}\right] \Bigg\} \\ &- \Gamma \rho_0 \frac{\epsilon_0}{t_0}[tH(t) - (t - t_0)H(t - t_0)]\end{aligned} \tag{25}$$

For comparison, the expression for stresses when the total energy ϵ_0 is deposited instantaneously is given as

$$\begin{aligned}\sigma(x, t) = \Gamma \rho_0 \epsilon_0 \Bigg\{ &H\left[t - \frac{(x + h/2)}{U_0}\right] \\ &+ H\left[t + \frac{(x - h/2)}{U_0}\right] - H(t) \Bigg\}\end{aligned} \tag{26}$$

A plot of the characteristics of the wave equation is shown in Fig. 9. The plot indicates the stress state in the plate for different regions in space-time. Expressions (25) and (26) are valid from $t = 0$ up until release waves are reflected.

Since we are interested in determining the conditions under which spallation occurs, and it has been shown that spallation will develop along the centerline $x = 0$, expression (25) is specialized for $x = 0$ and given as follows:

$$\begin{aligned}\sigma|_{x=0} = &- \Gamma \rho_0 \frac{\epsilon_0}{t_0}[tH(t) - (t - t_0)H(t - t_0)] \\ &+ 2\Gamma \rho_0 \frac{\epsilon_0}{t_0}\left[\left(t - \frac{h}{2U_0}\right) H\left(t - \frac{h}{2U_0}\right) \right. \\ &\left. - \left(t - t_0 - \frac{h}{2U_0}\right) H\left(t - t_0 - \frac{h}{2U_0}\right)\right]\end{aligned} \tag{27}$$

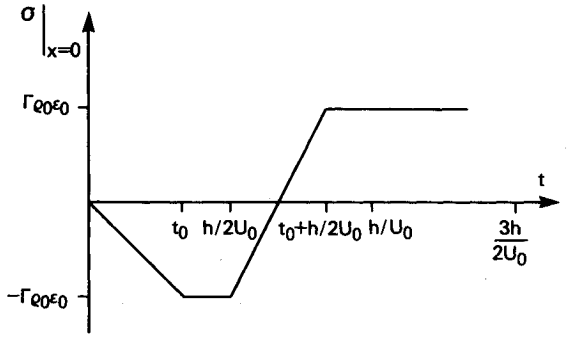

Fig. 10 Stress at plate centerline for $t_0 < h/2U_0$.

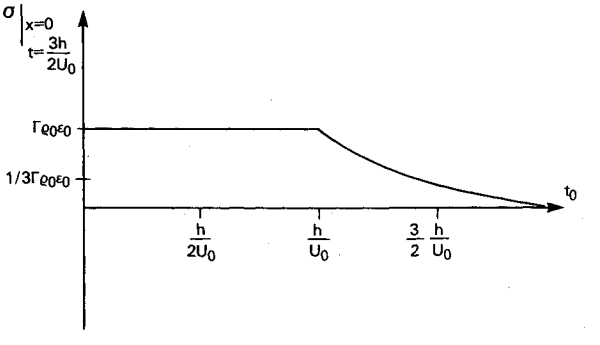

Fig. 11 Stress at plate centerline at critical time as a function of pulse length.

This expression can be used to determine stresses at the centerline of the material for a given value of t. Figure 10 shows the stress variation with time for cases in which $t_0 < h/2U_0$. As can be seen from the plot, the maximum tension and compression stresses are $\Gamma\rho_0\epsilon_0$ and $-\Gamma\rho_0\epsilon_0$, respectively. These are exactly the same stresses that were obtained during the consideration of instantaneous energy deposition. Thus, we can consider a material with energy deposited in a time $t_0 < h/2U_0$ to have the same response as if the energy was deposited instantaneously.

Under conditions in which the duration of the pulse is long, the maximum stress and the critical time for spallation to occur will be at $t = 3h/2U_0$. Therefore, using expression (26), maximum tensile stresses as a function of pulse duration can be found. The results of this are shown in Fig. 11.

Examples

To illustrate the use of the expressions derived in the previous sub-section, we will consider the response of an aluminum specimen of thickness 0.5 cm subjected to two different energy deposition rates. The parameters used in this example are as follows:

$$\rho_0 = 2.7 \text{ g/cm}^3$$

$$\Gamma = 2.1$$

$$E_0 = 68{,}900 \text{ MPa}$$

$$U_0 = \sqrt{E_0/\rho_0} = 0.51 \text{ cm}/\mu\text{s}$$

$$\sigma_{\text{ult}} = 520 \text{ MPa}$$

For the first case, we consider the energy deposited by the electron beam at NRL's Linac facility. The characteristics of this beam, which were given previously, are such that approximately 1 J/g is deposited for each pulse of duration 1.5 μs. Considering this energy to be deposited instantaneously through the material, maximum compressive and tensile stresses are computed from Eq. (26) and found to be

$$\Gamma\rho_0\epsilon_0 = 5.67 \text{ MPa}$$

However, as stated previously, the assumption of instantaneous energy deposition is valid for pulse lengths up to duration $h/2U_0$ which, for the case under consideration, is approximately 0.5 μs. Therefore, using expression (27), maximum tensile stress is computed to be 1.89 MPa. Thus, from this example it is obvious that spallation would not occur and that the assumption that the response of the material could be accurately described by its thermal effects alone was correct. As a second example, we consider a case in which 120 J/g are deposited in a pulse of 2.0 μs. If the incorrect assumption is made that the energy is deposited instantaneously, the resulting maximum tensile stress is approximately 689 MPa, which would lead one to believe that spallation failure, using the simplified criteria we have defined, is likely. However, if we consider the actual pulse duration as required by the established criteria, maximum tensile stresses would be 172 MPa, which is well below the spallation value.

The previous examples illustrate the effect that actual pulse duration has on computation of dynamic stresses. It is also seen that for anything other than disturbances of the shortest duration, relief waves propagating from the free surfaces will strongly diminish maximum stresses encountered in the material and a static situation is quickly reached.

Summary

The expressions and examples given here for determining the response of materials subjected to rapid in-depth heating have been intentionally simplified in order to obtain first-order estimates for assessing the importance of dynamic effects. Given the total energy deposited and deposition rates, maximum tensile stresses expected at a critical time and location ($t = 3h/2U_0$ and $x = 0$) can be computed and compared to a theoretical spallation strength. At stresses well below this value, it can be expected that dynamic effects will be insignificant.

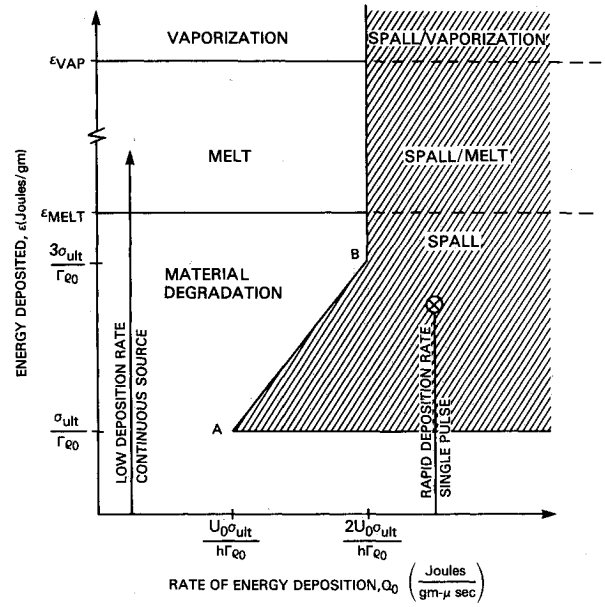

Fig. 12 Response diagram in terms of deposition rate and total energy.

Further work performed in this area should be directed toward assessing the effect that the initial assumptions made in the derivation would have on overall results. In particular, the assumption of linear constitutive relations should be studied. Also, if cases in which the surface area subjected to energy deposition is not large in comparison to material thickness are to be considered, the approach should be extended to two or three dimensions. Finally, it should also be pointed out that the analogous problem, for material subjected to surface energy deposition, should also be studied. The problem of energy absorption in a thin layer of an elastic half-space has been addressed in Ref. 11.

Conclusion

In this paper we have categorized the various directed energy weapons postulated under the Strategic Defense Initiative by the means in which they transfer energy to their target. Basic distinction is made between those in which energy is deposited on the surface and those that deposit energy through the thickness. Each of these categories is then subdivided by rate of energy deposition into categories denoted by slow and rapid.

Study of materials subjected to in-depth energy deposition indicated that for slow deposition, the material could be characterized by thermal response alone. Under these conditions, structural failure would be induced by a reduction in strength or stiffness of the material. It has been shown that thermal response of metals and composites can be found using numerical techniques in solving the nonhomogeneous heat conduction equation with temperature-dependent properties. Experiments that subjected aluminum, titanium, and graphite-epoxy specimens to electron-beam irradiation were used to verify the numerical results.

Material response due to rapid in-depth energy deposition is characterized by generation of extremely large stresses through the thickness of the material and possible failure by spallation. Calculation of the stress magnitudes was presented and shown to be straightforward if the energy is considered to be deposited instantaneously.

Since the response of materials is considerably different for the slow and rapid deposition cases, it is desirable to develop criteria that would indicate the dominant response. Simplified expressions based on total energy deposition along with deposition rate to determine stresses as a function of time and position through the plate have been developed. Using these expressions for a critical time and position, maximum tensile stresses are computed to determine if spallation would occur. If the stresses are significantly below the spallation strength, stresses will quickly dampen out, indicating that the material response can be characterized by thermal effects alone. With the information presented here, it is possible to develop a "response diagram" indicating the different mechanisms as a function of total energy and energy deposition rate. Such a diagram is shown in Fig. 12. The shaded area indicates regions in which spallation occurs. This region is then further divided, based on energy level, indicating whether the spalled material is a solid, liquid, or vapor. The unshaded area indicates regions where thermal response dominates. This area is also divided according to whether the material is vaporized, has melted, or remains as a solid but with reduced mechanical properties. Also, it can be seen from the figure that to induce spallation, point A represents the most efficient use of energy since it indicates the lowest total energy at the lowest deposition rate. For an aluminum plate of thickness 0.5 cm, which we have considered, this corresponds to 90 J/g with a pulse length of 1.0 μs. Point B represents the cutoff for determination of spallation in terms of deposition rate. That is, at all energy levels greater than $3\sigma_{ult}/\Gamma\rho_0$, or 270 J/g for our example, the minimum deposition rate required for spallation is $2U_0\sigma_{ult}/h\Gamma\rho_0$, or 180 J/g μs.

Although the "response diagram" presented here is based on the simplified expressions developed in this paper and is thus limited by the same assumptions, it does provide a visual means to determine material response characteristics due to varying rates of in-depth energy deposition.

Acknowledgments

The authors wish to acknowledge Dr. Phil Randles for his contribution to the development of stress wave expressions and also to H. N. Jones and G. W. Wissinger for providing the experimental results.

References

[1]Carter, A. B., "Directed Energy Missile Defense in Space," Office of Technology Assessment, OTA-BP-ISC-26, April 1984.

[2]Griffis, C. A., Chang, C. I., and Stonesifer, F. R., "Thermo-Mechanical Response of Tension Panels Under Intense Rapid Heating," *Theoretical and Applied Fracture Mechanics*, Vol. 3, 1985, pp. 41–48.

[3]Griffis, C. A., Masumura, R. A., and Chang, C. I., "Thermal Response of Graphite Epoxy Composite Subjected to Rapid Heating," *Journal of Composite Materials*, Vol. 15, Sept. 1981, pp. 427–442.

[4]Griffis, C. A., Nemes, J. A., Stonesifer, F. R., and Chang, C. I., "Degradation in Strength of Laminated Composites Subjected to Intense Heating and Mechanical Loading," *Journal of Composite Materials*, Vol. 20, May 1986, pp. 216–235.

[5]Carslaw, H. S. and Jaeger, J. C., *Conduction of Heat in Solids*, 2nd ed., Oxford, London, 1959.

[6]Dupuy, C. H. S., *Proceedings of the NATO Advanced Study Institute on Radiation Damage Processes in Materials*, Noordhoff International, the Netherlands, 1973.

[7]*American Institute of Physics Handbook*, 2nd ed., McGraw-Hill, 1963.

[8]Berger, M. J. and Seltzer, S. M., *Stopping Powers and Ranges of Electrons and Positrons*, 2nd ed., NBSIR 82-2550-A, Dec. 1982.

[9]McCracken, D. D. and Dorn, W. S., *Numerical Methods and Fortran Programming*, Wiley, New York, 1966.

[10]Touloukian, Y. S., Liley, P. E., and Saxena, S. S., *Thermophysical Properties of Matter*, IFI/Plenum, New York, 1970.

[11]Hegemier, G. A. and Morland, L. W., "Stress Waves in a Temperature-Dependent Viscoelastic Half-Space Subjected to Impulsive Electromagnetic Radiation," *AIAA Journal*, Vol. 7, Jan. 1969, pp. 35–41.